Shape transitions in soft spheres regulated by elasticity

Craig Fogle,[1] Amy C. Rowat,[2,3] Alex J. Levine,[1,4,5] and Joseph Rudnick[1]
[1]*Department of Physics, UCLA, Los Angeles, California 90095-1596, USA*
[2]*Department of Integrative Biology and Physiology, UCLA, Los Angeles, California 90095, USA*
[3]*Department of Bioengineering, UCLA, Los Angeles, California 90095, USA*
[4]*Department of Chemistry & Biochemistry, UCLA, Los Angeles, California 90095-1596, USA*
[5]*Department of Biomathematics, UCLA, Los Angeles, California 90095-1596, USA*
(Received 25 June 2013; published 11 November 2013)

We study elasticity-driven morphological transitions of soft spherical core-shell structures in which the core can be treated as an isotropic elastic continuum and the surface or shell as a tensionless liquid layer, whose elastic response is dominated by bending. To generate the transitions, we consider the case where the surface area of the liquid layer is increased for a fixed amount of interior elastic material. We find that generically there is a critical excess surface area at which the isotropic sphere becomes unstable to buckling. At this point it adopts a lower symmetry wrinkled structure that can be described by a spherical harmonic deformation. We study the dependence of the buckled sphere and critical excess area of the transition on the elastic parameters and size of the system. We also relate our results to recent experiments on the wrinkling of gel-filled vesicles as their interior volume is reduced. The theory may have broader applications to a variety of related structures from the macroscopic to the microscopic, including the wrinkling of dried peas, raisins, as well as the cell nucleus.

DOI: 10.1103/PhysRevE.88.052404 PACS number(s): 62.20.F−, 46.32.+x, 83.10.Ff, 62.23.St

I. INTRODUCTION

Euler buckling is a well-known mechanical instability. For a beam of length L under axial compressive loads, there is a critical compressive strain $\sim L^{-2}$ at which its deformation switches discontinuously from axial compression to the lateral deflection [1,2]. This mechanical instability and the breaking of the axial symmetry of the compressed beam by its lateral deflection provides a mechanical analogy to symmetry-breaking first-order phase transitions [3]. The role of Euler buckling in beams has, of course, been explored extensively in engineering and materials science [4], but it also plays an important role in biological physics in the context of buckling cytoskeletal filaments where such buckling affects force propagation along individual filaments [5] and the nonlinear mechanics [6,7] and structural evolution under load [8] of their networks.

Similar buckling and wrinkling instabilities appear in elastic sheets [9,10] under in-plane compressive stress. In cases where that compressive stress is generated by the growth or addition of material to a constrained system, morphological transitions induced by buckling result [11–14], and these are believed to have biological relevance in a variety of contexts, including the formation of fingerprints [15] and intestinal structures—villi and crypts—that can be reproduced *in vitro* [16] and understood theoretically [17] by considering the buckling of a thin elastic and growing layer coupled to a thick elastic substrate. More generally, the appearance of wrinkling of a stiff thin elastic layer mechanically coupled to a soft, three-dimensional elastic substrate has been studied quite generally [18–21] as has that of thin elastic layers coupled to a fluid substrate [22,23]. The modifications of the buckling phenomenon arising from coupling the elastic sheet to the substrate are generically twofold. First, the coupling increases the critical load at which buckling first occurs, and, second, it modifies the wavelength of the buckled state near the transition. The latter effect can be understood by noting that longer-wavelength buckling lowers the elastic energy of the thin sheet but generates deformations over longer length scales within the substrate at the cost of greater elastic energy there. The competition between these two elastic energies associated with the sheet and the substrate generate a minimum-energy buckled state at some intermediate wavelength. Without that competition, the buckling wavelength is controlled entirely by the system size, as it is in the archetypal case of Euler buckling in beam.

Morphological transitions can also be induced in compact elastic bodies, including a variety of core-shell structured spheres. In this article, we explore the surface wrinkling of a spherical elastic object bounded by a membrane, which supports bending stresses. Motivated primarily by the observation surface buckling of a giant unilamellar vesicle filled with an elastic gel as their interior gel was osmotically shrunk [24], we examine theoretically morphological transition driving by an increase in the surface area of the membrane-bounded sphere for fixed interior content. For sufficiently small amounts of excess area, the system simply expands isotropically. At a critical value of the excess area, however, the sphere buckles into a lower symmetry shape. We have determine the critical excess area and optimally buckled shape within a linear elastic analysis. More broadly, these results should be relevant to morphological transitions in a number of elastic core-shell structures [25] and even the cell nucleus [26].

The remainder of the article is organized as follows. In Sec. II A we, first, present the results of a heuristic model replacing the interior elastic deformation field with a scalar Laplacian model. This theory provides insight into the single control parameter for the morphological transition and the basic competition between the elastic energy cost of surface deformation favoring buckling at longer wavelengths and interior strain favoring buckling at shorter wavelengths. In Sec. II B we present the full elastic calculation. In Sec. III we examine the solution and analyze the first-order buckling

transition and determine the dominant deformation mode in the buckled state. We find a first-order transition to a buckled state identified as a spherical harmonic mode $Y_{\ell m}$ with $\ell \sim \mathcal{O}(10)$ for a broad range of the relevant elastic parameters and $m = \ell$, although there are typically generated m states for larger ℓ. Finally, we conclude in Sec. IV with a discussion of the implications of these results to current experiments and proposals for future tests. A few details of a more technical nature are relegated to the appendix.

II. THE MODEL

A. Scalar model

It is helpful to first examine a heuristic model that dramatically simplifies the elastic calculation of the interior of the sphere but still manages to capture the basic competition between surface and bulk elastic energies. To that end we replace the vectorial elastic displacement field $\mathbf{u}(\mathbf{x})$ by a scalar field $\phi(\mathbf{x})$ that obeys the Laplace equation rather than the usual equation of stress continuity in a bulk elastic medium. In this way we neglect the distinction between transverse and longitudinal modes of the solid but retain the basic power counting of derivatives in the equation of stress continuity, which is necessary for our argument. We impose "excess area" on the surface of the elastic sphere of radius R by requiring the scalarized deformation to be given there by

$$\phi(r = R,\theta) = \Phi P_\ell(\cos\theta), \tag{1}$$

where P_ℓ is a Legendre polynomial and θ is the polar angle. In this way we impose a deformation on the surface in the form of a spherical harmonic. In the scalarized approach we specialize to azimuthally symmetric modes ($m = 0$) but this is not essential and is relaxed in the full calculation presented below. The surface deformation can be thought of as being imposed by a set of normal stresses on the sphere's surface that serve as a method for injecting excess area on the surface. The morphological transition can be understood as resulting from either imposing excess surface area or reducing the interior volume of the unstrained material. For example, shape transitions are observed when gel-filled vesicles are osmotically shrunk [24]. In either case, the application of surface stresses is equivalent to changing the reference state within linear elasticity theory—see Appendix A for a more detailed discussion.

Given that $\phi(\mathbf{x})$ satisfies the Laplace equation, a solution satisfying the above condition is given in terms of the polar angle θ and radial distance r from the origin of the coordinate system at the center of the sphere by

$$\phi(r,\theta) = \Phi\left(\frac{r}{R}\right)^\ell P_\ell(\cos\theta). \tag{2}$$

The deformation energy of the elastic interior is

$$E_{\text{bulk}} = \frac{\gamma}{2}\int_{r<R} d^3\mathbf{x}(\nabla\phi)^2, \tag{3}$$

where γ is the single elastic constant in the scalarized elastic model, which has dimensions of energy per length. Inserting the solution Eq. (2) into Eq. (3), we find that

$$E_{\text{bulk}} = 2\pi\gamma R\Phi^2\left[\frac{1+\ell(\ell+1)}{(2\ell+1)^2}\right]. \tag{4}$$

The prefactors associated with the elastic constant, sphere's radius, and magnitude of deformation follow naturally from dimensional analysis; the

ℓ-dependent term in square brackets, however, shows that higher-order spherical harmonics (of the same amplitude) generate less elastic energy storage in the interior. In terms of the energy of the $\ell = 0$ mode $E_0 = 2\pi\gamma R\Phi^2$, the elastic energy associated with the ℓ^{th} mode decays monotonically with ℓ to the limiting value of $E_{\text{bulk}} \to \frac{E_0}{4}$ as $\ell \to \infty$.

We now introduce a bending energy associated with the surface deformation imposed by $\phi(\mathbf{x})$, specified in Eq. (1). Letting $\nabla_\perp$ be the parts of the gradient operator normal to the radial direction, we approximate this bending energy as

$$E_{\text{surf}} = \frac{\tilde{\kappa}}{2}R^2\oint_{r=R} d\Omega[\nabla_\perp^2\phi]^2, \tag{5}$$

where $\tilde{\kappa}$ is the bending energy, which, in the scalarized model, has dimensions of length squared times energy. This form of the bending energy is correct only for small deformations from an originally flat surface, so it is approximate in this case and can be justified only *a posteriori* by showing that the energy-minimizing buckling wavelength is small compared to the sphere's circumference; see below. In the full calculation, shown in the next section, such approximations are not used. Using the solution Eq. (2) we find the bending energy to be given by

$$E_{\text{surf}} = \frac{2\tilde{\kappa}\pi\Phi^2}{R^2}\left[\frac{\ell^2(1+\ell)^2}{2\ell+1}\right]. \tag{6}$$

The sum of the energetic contributions from the bulk Eq. (4) and the surface Eq. (6) give the total energy cost of a given deformation in mode ℓ, E_ℓ. To determine the minimum such energy for a given *excess surface area* ΔA, we first compute the "excess area" associated with the deformation ϕ,

$$\Delta A = \frac{R^2}{2}\oint d\Omega[\nabla_\perp\phi]^2, \tag{7}$$

and use this result to eliminate the amplitude of the deformation field Φ in favor ΔA. Defining a dimensionless energy $\mathcal{E}_\ell = R^2E_\ell/2\pi\tilde{\kappa}$ we find that the energy of a deformation in the Y_ℓ^0 mode generating excess surface area ΔA is given by

$$\mathcal{E}_\ell = \frac{\Delta A}{\ell(\ell+1)}\left[\tilde{\alpha}\frac{1+\ell(\ell+1)}{2\ell+1} + \ell^2(\ell+1)^2\right], \tag{8}$$

where we have introduced a single dimensionless control parameter,

$$\tilde{\alpha} = \frac{\gamma R^3}{\tilde{\kappa}}. \tag{9}$$

This dimensionless constant describes the relative stiffness of the interior as compared to the surface. For large ℓ one notes that the dimensionless energy in Eq. (8) is given roughly by

$$\frac{\mathcal{E}_\ell}{\Delta A} \sim \frac{\tilde{\alpha}}{\ell} + \ell^2, \tag{10}$$

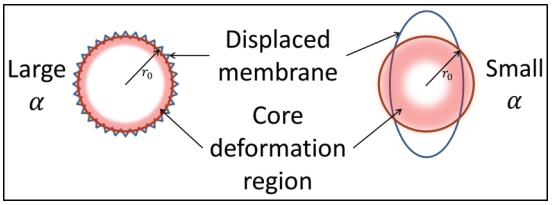

FIG. 1. (Color online) A schematic representation of the basic energy balance between the surface and the bulk. By inserting excess surface area in a short wavelength deformation as shown on the left, the deformation field in the interior decays rapidly, minimizing bulk elastic energy at the cost of the incurring high bending energy on the surface. Inserting the same excess area into a lower spherical harmonic, as shown on the right, exchanges the relative importance of surface and bulk energetic contributions. This trade-off between bulk and surface energy selects a optimally buckled state with $\ell \sim \alpha^{1/3}$. See text for details.

showing that a minimum exists for a mode at

$$\tilde{\ell}^{\star} \sim \tilde{\alpha}^{1/3}. \tag{11}$$

The key features determining the form of Eq. (10) can be readily understood. The $\frac{\tilde{\alpha}}{\ell}$ and ℓ^2 represent the energetic contribution from the interior and the surface, respectively. The growth of $\mathcal{E}_\ell$ at large ℓ reflects the high bending energy cost of the high ℓ modes, but the first term, weighted by the ratio of the bulk to surface modulus, decreases with increasing ℓ. The deformation field in the sphere's interior becomes confined to a type of boundary layer: $\phi \sim (r/R)^{\ell}$. Figure 1 shows a schematic representation of this trade-off between the confinement of the interior strain to a boundary layer at high ℓ, leading to the reduction of the bulk energy and the monotonically growing bending energy cost of injecting a fixed amount of excess surface area into a mode with increasing ℓ.

The qualitative features of this result will survive the introduction of a proper vectorial displacement field to describe the deformation state of the sphere. In that case, we will replace the dimensionless control parameter $\tilde{\alpha}$ by

$$\alpha = \frac{\mu R^3}{\kappa}, \tag{12}$$

where μ is the shear modulus of the bulk and κ is the bending modulus of the surface. Ignoring a weak dependence on the Poisson ratio of the bulk elastic material, we will find a similar structure of the total energy, yielding a transition from a spherical state to deformation in the mode $\ell^{\star}$. The generic nature of the result is not surprising in light of previous work on buckling of beams embedded in an elastic medium [27]. In that case, the beam is generically stiffened against buckling by the surrounding medium and the unstable mode associated with the buckled state shifts from the lowest wavelength allowed by the length of the beam to a finite wavelength set by the ratio of the beam's bending modulus and the elastic constants describing the surrounding medium [27]. The finite wavelength results from the fact that the continuum elastic theory is Laplacian. Undulations of the beam at wave vector k generate strain in the elastic continuum that decays over a distance $1/k$ into the medium. This sets up the same trade-off between beam bending energy and bulk elastic energy as discussed here. The key differences in the present calculation involve the spherical geometry of the undeformed structure, which renders the calculation more difficult.

B. Full elastic calculation

To calculate the energy associated with the membrane bounding the elastic sphere we introduce the Helfrich energy of that surface that depends on the mean curvature H, the spontaneous curvature $H_s = 2/R_s$, and a single elastic constant, the bending modulus κ,

$$E_{\text{surface}} = \frac{\kappa}{2} \oint_{r=R} R^2 d\Omega (H - H_s)^2, \tag{13}$$

where the integral is over all solid angles. Since we consider only genus-preserving morphological transitions, we may neglect terms proportional to the Gaussian curvature modulus [28].

To determine the elastic energy stored in the sphere's interior, we parameterize the strain in the usual way by introducing the symmetrized deformation tensor $u_{ij} = (1/2)[\partial_i u_j + \partial_j u_i]$ calculated from the displacement field $\mathbf{u}(\mathbf{x})$ defined everywhere within the undeformed body, a sphere of radius R. The elastic properties of the interior are described in terms its shear modulus $\mu > 0$ and the Poisson ratio $-1 < \nu < 1/2$, with $\nu = 1/2$ corresponding to an incompressible solid. In terms of these parameters the elastic energy associated with a given deformation state of the sphere is given by [2]

$$E_{\text{bulk}} = \mu \int_{|\mathbf{x}|<R} d^3x \left(\frac{\nu}{1-2\nu} u_{ii}^2 + u_{ij}^2 \right). \tag{14}$$

The integral is over the reference space of the undeformed sphere. The above strain tensor satisfies the standard stress continuity equation $\partial_i \sigma_{ij} = 0$ within the sphere requiring that $\mathbf{u}$ satisfy

$$\frac{1}{1-2\nu} \nabla \nabla \cdot \mathbf{u} + \nabla^2 \mathbf{u} = 0. \tag{15}$$

The total energy of deformation, which is the sum of the contributions from Eqs. (13) and (14) is fully determined once one requires that the state of deformation of the elastic interior matches the imposed normal displacements at its boundary surface, $r = R$. To do that we require that the normal displacements obey

$$\mathbf{u}(R,\theta,\phi) \cdot \hat{\mathbf{r}} = R g(\Omega), \tag{16}$$

with $\Omega = (\theta,\phi)$ representing the polar and azimuthal angles. Since we consider a fluid membrane boundary and look at static states of deformation, the tangential displacements of the elastic core $\mathbf{u}_\perp(r = R,\Omega)$, $\mathbf{u}_\perp \cdot \hat{r} = 0$ do not affect the deformation energy of the surface. We take these displacements to be zero for now and return to this point later in the discussion.

Following the analysis of the heuristic model above, we impose a deformation on the surface of the sphere so the radial distance $r(\Omega)$ from its center to the deformed boundary is expanded in spherical harmonics [29]. In other words,

$$r(\Omega) = R[1 + g(\Omega)] = R \left[1 + \sum_{\ell,m} g_{\ell m} Y_{\ell m}(\Omega) \right]. \tag{17}$$

In order to make the radial deformation of the sphere explicitly real, we have introduced linear combinations of the complex spherical harmonics Y_ℓ^m for $m > 0$,

$$Y_{\ell m} = \tfrac{1}{\sqrt{2}}\left[Y_\ell^m + (-1)^m Y_\ell^{-m}\right], \tag{18}$$

and set $Y_{\ell 0} = Y_\ell^0$ for the azimuthally symmetric mode. Other linear combinations of the spherical harmonics of the form $Y_\ell^m e^{im\phi_0} + (-1)^m Y_\ell^{-m} e^{-im\phi_0}$ correspond to the same deformation state but simply rotated azimuthally by ϕ_0. As such, they are not interesting, at least until one considers the energy cost of linear combinations of such deformation modes. Finally, it will prove convenient to rescale the amplitude the $\ell = 0$ mode by introducing the notation $\bar{g}_0 = g_0/\sqrt{4\pi}$.

Since the surface energy Eq. (13) is quadratic in the deformations, the spherical harmonic decomposition of the surface deformation energy yields a result quadratic in amplitudes $g_{\ell m}$ for $\ell \neq 0$,

$$\begin{aligned} E_{\text{surface}} = {} & \bar{E} + 2\pi\kappa\bar{g}_0\omega_s[\omega_s(2+\bar{g}_0) - 2] \\ & + \frac{\kappa}{8}\sum_{\ell\neq 0,m} g_{\ell m}^2[\ell(\ell+2)(\ell^2-1) - 4\omega_s\ell(\ell+1) \\ & + 2\omega_s^2(\ell^2+\ell+2)], \end{aligned} \tag{19}$$

where $\omega_s = R/R_s$ is the ratio of the undeformed sphere's radius to the spontaneous curvature of its bounding membrane and $\bar{E} = 2\pi\kappa(1-\omega_s)^2$ is the energy associated with the mismatch ($\omega_s \neq 1$) between these quantities.

Such a mismatch $\omega_s \neq 1$ leads to a "prestress" in the membrane-sphere system due to the incompatibility of their undeformed states. We do not explore these effects here, but it is clear that the prestress above can lead to buckling at zero excess area.

We may also calculate change in surface area associated with the deformation of the sphere. Keeping terms to $\mathcal{O}(g^2)$, we find

$$\frac{A}{4\pi R^2} = (1+\bar{g}_0)^2 + \frac{1}{8\pi R^2}\sum_{\ell\neq 0,m} g_{\ell m}^2[\ell^2+\ell+2]. \tag{20}$$

The first term is the extra area associated with the uniform change in the sphere's radius, i.e., the $\ell = 0$ mode. The second term gives the contributions from all the higher modes of deformation $\ell > 0$. Both the results for the bending energy and contribution to the surface area are consistent with previous work on the undulations of micelles [29]. In the following we will consider the fractional excess area Δ of the deformed sphere as the control parameter for the transition from spherical to deformed shapes. Consequently, we define

$$\Delta = \frac{A}{4\pi R^2} - 1. \tag{21}$$

The surface energy Eq. (19) and the excess area Eq. (20) both take the form of sums of terms each proportional to the square of the spherical harmonic mode amplitudes. This will also be true of the elastic energy stored in the sphere's interior [Eq. (14)]. Thus, in a deformation state given by a linear combination of such modes, the contributions of each mode to both the energy cost and excess surface area are simply additive. For this reason it is sufficient to consider a single spherical harmonic mode at a time.

The remaining calculation of the energy stored in the elastic interior is somewhat tedious; we present the key features of the calculation here and the remaining details in Appendix B. Our method of solution has been used to consider the deformations of spherical inclusions embedded in another elastic medium [30], but we consider the problem with displacement, rather than stress, boundary conditions at the surface. To briefly describe the approach: If one were to obtain a harmonic vector $\mathbf{S}_{\ell m}(\mathbf{x})$, i.e., $\nabla^2\mathbf{S} = 0$. that matches the boundary conditions imposed on the displacement field at the boundary $r = R$ so $\mathbf{S}(r = R,\Omega) = \hat{\mathbf{r}} g_{\ell m} Y_{\ell m}(\Omega)$, then a displacement field of the form

$$\mathbf{u}(\mathbf{x}) = M_\ell(R^2 - r^2)\nabla\nabla\cdot\mathbf{S}_{\ell m} + \mathbf{S}_{\ell m}, \tag{22}$$

with

$$M_\ell = \frac{1}{4(1-\nu)(2\ell-1) - 2\ell} \tag{23}$$

is a solution to Eq. (15) with the correct boundary conditions, as may be checked by direct computation.

Recognizing that $Y_{\ell m}$ is a linear combination of complex spherical harmonics $Y_\ell^{\pm m}$, it is sufficient to produce a complex harmonic vector field $\mathcal{S}$ that generates the appropriate part of the radial displacement at the surface,

$$\mathcal{S}(r = R,\Omega) = \hat{\mathbf{r}} Y_\ell^m(\Omega). \tag{24}$$

The Cartesian components of such a complex vector are products of $\hat{r}\cdot\hat{e}_i$, $i = x,y,z$, and Y_ℓ^m. Using the usual rules for adding angular momentum, such products can be expanded in spherical harmonics having $\ell' = \ell-1,\ell,\ell+1$ and $m' = m-1,m,m+1$ with coefficients given by the Clebsh-Gordon coefficients. The net result is a displacement field that gives the appropriate radial displacement on the surface in a single $Y_{\ell m}$ mode but contains a sum of terms including that mode as well as modes with $\ell \pm 1$ (and $m \pm 1$) in the interior. Taking the necessary derivatives, one obtains the strain tensor and, from that, the elastic energy density. Integrating the energy density over the volume of the sphere, we obtain the total bulk elastic energy. That result, combined with Eqs. (19) and (20), completes our analysis of the geometry and energetics of the sphere held in a deformed state. As in the heuristic example, it is necessary only to eliminate the amplitude of the surface deformation in favor of the true control variable, the excess area [using Eq. (20)]. For a deformation consisting of a single harmonic with ℓ this leads to

$$g_{\ell m}(\Delta) = \begin{cases} \sqrt{4\pi}\left(\sqrt{1+\Delta}-1\right) & \text{for} \quad \ell = 0 \\ \sqrt{\Delta}\left(\frac{8\pi}{\ell(\ell+1)+2}\right)^{1/2} & \text{for} \quad \ell \neq 0 \end{cases}, \tag{25}$$

where the fraction excess area Δ is defined by Eq. (21).

For small Δ, the amplitude of the $\ell = 0$ mode grows as $g_{00} \sim \Delta$. For all other modes with $\ell > 0$ the amplitude grows as $g_{\ell m} \sim \Delta^{1/2}$. Since the deformation energies of both the surface and the bulk are proportional to g^2 (when $\omega_s = 1$, i.e., no prestress), the energy cost for inserting the the excess area into the $\ell = 0$ mode grows as Δ^2. For the $\ell > 0$ modes, however, it grows linearly.

Thus, for sufficiently small Δ, the isotropic deformation is necessarily lower in energy. At some ℓ- and m-dependent values of the excess area, the energetic cost storing that

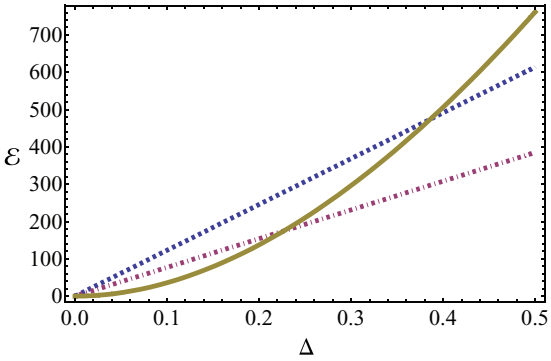

FIG. 2. (Color online) The dimensionless energy $\mathcal{E} = E/\kappa$ of the deformed sphere and membrane as a function of the fractional excess area Δ for isotropic growth $\ell = 0$ solid (gold) and for buckling into the $\ell = 8, m = 0$ dashed (blue) mode or the $\ell = 8, m = 8$ dot-dashed (purple). The dimensionless control parameter is $\alpha = 575$ and the Poisson ratio of the interior is $\nu = 0.2$. As discussed in the text, the $\ell = 8, m = 8$ mode is the minimum energy buckled state of the sphere. The transition from isotropic expansion to buckling occurs at $\Delta \approx 0.22$.

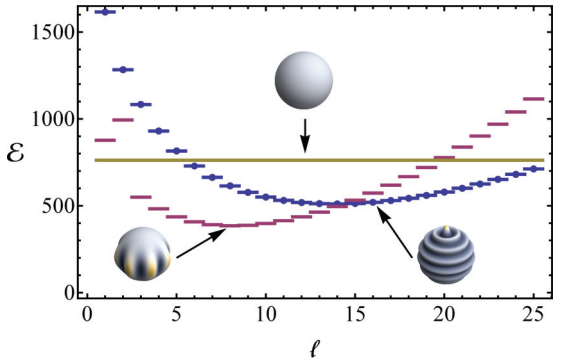

FIG. 3. (Color online) Plot of the dimensionless energy $\mathcal{E} = E/\kappa$ vs the angular harmonic of the buckled state ℓ for $\alpha = 575$, $\nu = 0.2$ and fixed fractional excess area $\Delta = 0.5$. These plots can be used to determine the optimal buckled state symmetry $\ell^\star$. The solid (gold) line shows the energy of the isotropically expanded state. The dashed (red) curve gives the energies of the $\ell = m$ state and the dot dashed (blue) curve the energies of the $m = 0$ state at each ℓ. For this α, ν combination the lowest energy configuration at $\Delta = 0.5$ is given by $\ell = m = 8$. Representative figures of the isotropic state (top), the $\ell = m = 8$ state (bottom left), and the $\ell = 16, m = 0$ (bottom right) are shown.

excess area in these finite ℓ modes must become lower than storing it in the isotropic one. At that point a morphological transition results. This is illustrated in Fig. 2, which shows the nondimensionalized energy of the system $\mathcal{E} = E/\kappa$ as a function of the fractional excess area Δ [see Eq. (21)] in three cases: Accommodating that excess area by isotropically expanding the sphere and membrane system (sold line, gold) or by creating a lower symmetry buckled state in the $\ell = 8, m = 0$ (dashed line, blue) or $\ell = 8, m = 8$ (dashed dotted line, purple) mode. It is clear that there is a transition near $\Delta^\star \simeq 0.22$ where the isotropic solution is no longer the energy-minimizing solution.

As with the heuristic toy model, α [see Eq. (12)] is the key dimensionless parameter controlling both the fractional critical excess area of the transition $\Delta^\star$ and the symmetry of the optimally buckled state above the transition $\ell^\star$. The Poisson ratio of the elastic material inside the sphere has a weak effect on the quantitative results as long as $\nu < 1/2$, i.e., as long as the material is not restrictly incompressible. We return to this point in the next section. Of the three cases shown, the optimal solution is the $\ell = 8, m = 8$ one; it will be shown later that, for these parameters giving $\alpha = 575$ and $\nu = 0.2$, there are in fact six degenerate optimal solutions with $\ell = 8$ and $m = 3, \ldots, 8$. In the next section we survey the dependence of the buckling transition on α, examine the buckled state more closely, and present an overall phase diagram of core-shell buckling.

III. RESULTS

Having seen that a buckling transition is required from a basic scaling analysis, we examine in more detail which buckled configuration is an energy minimum and which material parameters control the symmetry of the optimally buckled shape. To determine which is the optimally buckled shape above the transition, i.e., for $\Delta > \Delta^\star$, we plot the dimensionless energy $\mathcal{E}$ as a function of the angular harmonic ℓ, using the same values of the material parameters as above ($\alpha = 575$ and $\nu = 0.2$). A representative example is shown in Fig. 3 in which the energy of the buckled sphere is plotted for buckling mode $\ell, m = 0$ (dashed dot, blue) and $\ell, m = \ell$ (dashed, purple). For comparison, we show the energy of the isotropically expanded state as a solid (gold) line. In all cases the fractional excess area is fixed at $\Delta = 0.5 > \Delta^\star \simeq 0.22$, so some lower symmetry state of the system is the energy minimum. Here, we see that the $\ell^\star = 8$ state with large m is the lowest energy buckled state of the system. We will find that the larger m solutions for a given ℓ are, in fact, generically of lower energy.

Repeating this exercise for various values of α, one determines both the dependence of the critical fractional excess area $\Delta^\star$ and the symmetry of the minimum energy buckled state $\ell^\star$ on the control parameter α. The results for the dependence of $\ell^\star$ on α are shown in Fig. 4 for two different values of the fractional excess area: $\Delta = 0.4$ dashed (blue) and $\Delta = 0.25$ solid (red). As expected based on the heuristic model, we find that $\ell^\star \sim \alpha^{1/3}$, as shown by a comparison to the cube root function dashed by the dashed line in the figure. For sufficiently small values of α the interior of the sphere is too compliant to drive the buckling transition; the isotropic deformation of the sphere is the energetically favored manner of storing the excess surface area. Collecting more results of this form, we observe that the critical fractional excess area decreases with increasing α for fixed Poisson ratio as $\Delta^\star \sim \alpha^{-1/3}$, as is discussed later in terms of the overall buckling phase diagram.

The dependence of these results on the Poisson ratio is generically weak (see Fig. 5), except in the singular limit of $\nu \to 1/2$ where the material becomes incompressible. As ν approaches $1/2$, the symmetry of the optimally buckled state is gradually reduced. A more incompressible interior results in more wrinkles for the buckled state. As expected, the energy cost of the isotropically expanded sphere increases without bound as the sphere's interior is made more incompressible. Consequently, the critical value of the excess fractional area

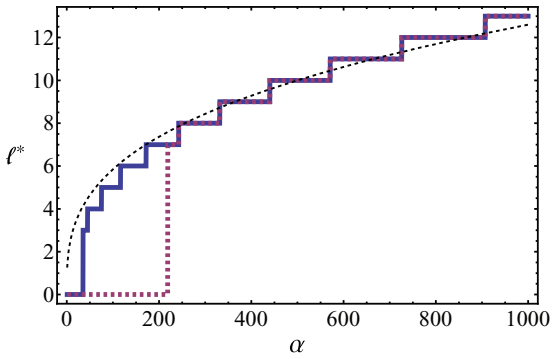

FIG. 4. (Color online) Plot of $\ell^\star$, the angular harmonic of the minimum energy state of the sphere as a function of α for fixed fractional excess areas $\Delta = 0.25$ dashed (purple) and $\Delta = 0.4$ solid (blue). For sufficiently soft interiors (small α) the isotropic shape is the energy minimum. As α is increased, the sphere transitions to a buckled state with $\ell^\star$ and $m = \ell^\star$. As expected from the heuristic treatment of scalarized elasticity, symmetry of the optimally buckled state $\ell^\star \sim \alpha^{1/3}$, as shown by the dashed (black) line.

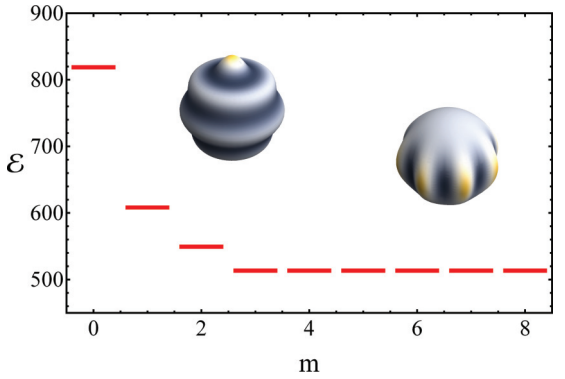

FIG. 6. (Color online) Example of the degeneracy of the buckled state energy with respect to m for a representative value of $\ell = 8$ and $\alpha = 575, \nu = 0.2$ and excess fractional area of $\Delta = 0.5$. For fixed ℓ the energy initially decreases with m until $m = 3$. All states with $m \geqslant 3$ are generate. Superposed on the plot are pictorial representations of the higher energy state with $m = 0$ (left) and one of the lowest energy states with $m = \ell = 8$ (right).

Δ decreases continuously with increasing ν. Finally, at $\nu = 1/2$, the isotropic solution is disallowed by the compressibility condition and buckling occurs for all $\Delta > 0$ and all α.

When examining the energy of various buckled states for the same ℓ, one notes that it is a nonincreasing function of m. The buckled states having rings of equal radial deformation extending azimuthally around the sphere, e.g., the $m = 0$ state is always the highest energy state with the subspace of equal ℓ buckled configurations. As m is increased, the energy initially decreases within increasing m but reaches a plateau for $m \geqslant 3$ independent of ℓ for $\ell > 3$. An example of this degeneracy is shown in Fig. 6 for the $\ell = 8$ with the same combination of α, ν as used in the previous figures. The fractional excess surface area is fixed at $\Delta = 0.5$.

This degeneracy can be understood as follows. Referring to Appendix B, we see that the displacement field in the sphere's interior associated with a surface deformation proportional to $Y_{\ell m}$ contains terms with angular dependence given by a sum of spherical harmonics with $m - 1, m, m + 1$. The

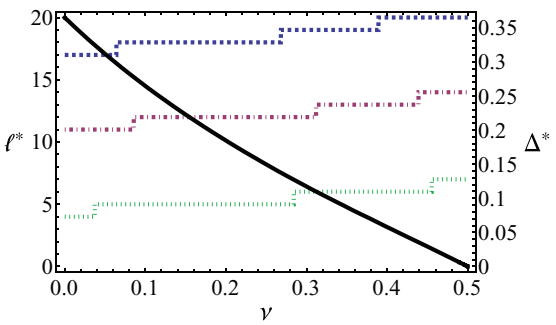

FIG. 5. (Color online) Plot of $\ell^\star$, the angular harmonic of the minimum energy state of the sphere as a function of ν for $\alpha = 100, 800, 2500$: dotted (green), dash-dotted (purple), and dashed (blue), respectively. As the interior is made less compressible, the optimally buckled shape has lower symmetry, i.e., higher $\ell^\star$ (left axis). Additionally, the critical fractional excess area $\Delta^\star$ (black line, right axis) decreases continuously to zero as $\nu \to 1/2$, the incompressible limit, for fixed $\alpha = 575$.

elastic energy density requires one more spatial gradient of $\mathbf{u}(\mathbf{x})$. Since the gradient is a vector operator, the resulting elastic energy density will contain a sum of terms having magnetic quantum numbers of $m - 2, \ldots, m + 2$. Recall also our spherical harmonics $Y_{\ell m}$ are superpositions of complex spherical harmonics with $\pm m$ so the volume integral of the bulk energy density contains an array of products of terms having magnetic quantum numbers between $-m - 2, \cdots - m + 2$ and $m - 2, \ldots m + 2$. Cross products between these two sets of terms vanish on integration unless the sum of their magnetic quantum numbers vanishes. There are more such nonvanishing products, however, if these two sets of terms have an overlap; in other words, if $m \leqslant 2$, then there is an accessible solution to $-m + 2 = m - 2$ and more products are nonvanishing in the computation of the internal energy of the sphere. These terms necessarily make a positive contribution to the elastic energy of the sphere since every deformation adds to the elastic energy. Thus, as m is increased, the number of these cross terms is reduced as the total elastic energy of deformation decreases. Once $m \geqslant 3$, however, there are no more cross terms. The higher m deformations are now degenerate, at least within the linear elastic theory. Nonlinear elastic terms in the sphere's interior or surface compression energies (we include only bending) probably lift this degeneracy, but such effects are beyond the scope of the current analysis.

The physical effect of these extra terms in the energy density is well illustrated by plotting the distribution of elastic energy storage in two spheres with $\ell = 8$ surface deformations. Their energy densities are shown as a heat map in Fig. 7 for the $m = 0$ (left) and the $m = 8$ (right) solutions. The $m = 0$ mode is clearly higher in energy, as can be seen by noting the difference between the two color scales. From a comparison of the two figures, it is clear that in both cases the elastic deformation energy is confined to a boundary layer near the sphere's surface, as expected based on the heuristic calculation. In the $m = 0$ solution, however, there is a distinct concentration of the elastic energy near the sphere's poles. This is due to the fact that $m = 0$ distortion lay along lines of longitude. Near the poles these undulatory rings of deformation become tightly

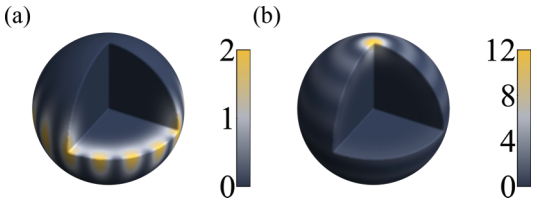

FIG. 7. (Color online) A comparison of the distribution of the elastic energy density in spheres having the same fractional excess area $\Delta = 0.5$ and same elastic parameters $\alpha = 575, \nu = 0.2$. On the left (a) the excess area is put into the $\ell = 8, m = 8$ mode. Here the energy density is primarily spread out over the equator. On the right (b) the excess area is put into the $\ell = 8, m = 0$ mode so the sphere's surface has undulatory rings that run along lines of constant latitude. The overall elastic energy of A is less than that in B; note the difference in the energy scale associated with the two color maps.

wrapped. In the $m = 8$ solution the elastic energy is spread out primarily over the equator of the sphere, resulting in a lower total energy.

Putting these results together into a more unified picture, we present a phase diagram for spherical elastic core–membrane shell structures in Fig. 8. The diagram is spanned by the excess fractional area Δ and the control parameter α for a fixed value of the Poisson ratio $\nu = 0.2$. This phase diagram is representative of other ν values with the exception of the $\nu = 1/2$ incompressible case, as mentioned above. The solid black in Fig. 8 line divides the phase space of such elastic objects into

isotropic and expanded spheres below line and lower symmetry buckled ones above it. One also observes the dependence of the critical fractional excess area on α. As α is increased $\Delta^\star$ indeed decreases and the symmetry of the buckled state decreases as well. The angular harmonic of the optimal buckled state $\ell^\star$ is shown by the horizontal axis

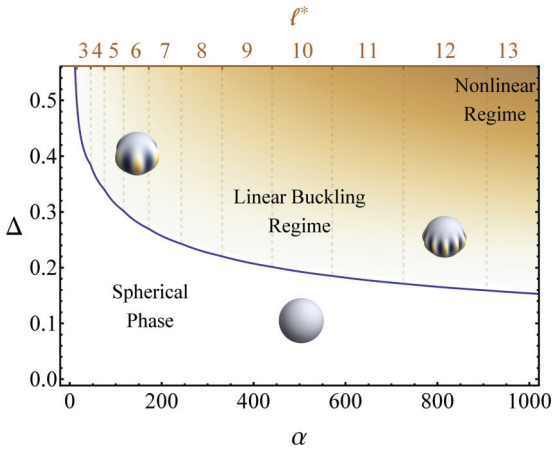

FIG. 8. (Color online) Buckling phase diagram of core-shell structures spanned by the fractional excess area Δ and the dimensionless control parameter α. The (solid, black) curve separates isotropically expanded spheres from lower symmery buckled states. As $\alpha = \mu R^3/\kappa$ is increased, the interior material stiffens relative to the bending modulus of the boundary, leading to buckling at smaller Δ. Also, as α is increased, the $\ell^\star$ of the buckled state near the transition also increases; see the top axis. Representative shapes for these minimum energy buckling spheres are shown for $\ell^\star = 6, 12$.

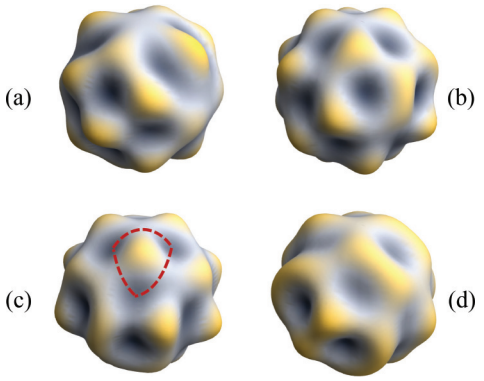

FIG. 9. (Color online) Examples of mixing the degenerate buckling modes for a system with $\mu = 0.2$ and $\alpha = 300$. For this value of the control parameter, the degenerate modes are the $\ell = 8$ and $m \in [3,8]$. Each example is an equally weighted mixture of buckling modes with amplitude such that $\Delta = 0.4$. (a) $m = 4$ and 6; (b) $m = 3$ and 7; (c) $m = 3$ and 8; (d) $m = 3$, 5, 7, and 8.

along the top of the figure. The representative figures show the $\ell = m$ state, which, as described earlier, is always part of the degenerate subspace of optimally buckled shapes for $\ell^\star \geqslant 3$. Such buckled shapes are qualitatively similar to the buckled gel-filled vesicles of Refs. [24,31].

There are a variety of other buckled core-shell structures. In particular, Cao and coworkers investigated the buckling of Ag core–SiO_2 shell particles experimentally [32] and numerically [25], where, relying the materials' differential thermal expansion, buckling was induced by temperature change. In these systems, a triangular pattern of ridges was observed near the transition from the smooth spherical state, while, deeper in the buckled phase, labyrinthine patterns were observed. The triangular patterns observed near the transition have lower symmetry than the single spherical harmonic mode predicted by the linear theory. Such triangular patterns, however, can be simply reproduced from our results by forming a linear superposition of the degenerate buckling modes predicted herein. This is shown in Fig. 9, where we reproduce examples of lower symmetry buckling states by combining degenerate buckling modes all with $\ell = 8$. One generically finds a triangular pattern of dimples in such cases, as shown by the dashed (red) line in Fig. 9(c). Understanding whether these mixed modes truly represent lower energy solutions or are the result of some underlying quenched disorder in the core-shell system is beyond the scope of our linear elasticity approach. Nevertheless, from our analysis it is easy to see that either small elastic nonlinearities or disorder may select such mixed modes from the space of degenerate states that we identify and that these mixed mode solutions are qualitatively similar to those observed.

IV. SUMMARY

We have demonstrated the analog of Euler buckling in spherical core-shell structures where the shell is treated as a tensionless lipid membrane, i.e., one whose elasticity is controlled solely by a bending modulus, κ. Such systems are found in gel-filled vesicles, but with some modifications to the treatment of the surface elasticity of the bounding

membrane (e.g., adding an area compression modulus), these calculations have more general relevance to a variety of soft elastic solids coupled to thin shells, such as any number of colloidal core-shell particles [25,26,33–35] or even the blastocyst that transitions from spherical to ovoid shape during embryonic development [36]. Following our exploration of a heuristic scalarized elasticity theory, we identified one control parameter for the transition on increasing the bounding surface area between an isotropically expanded sphere and a buckled one. This control parameter $\alpha = \mu R^3/\kappa$ measures the relative compliance of the sphere's interior to its boundary. In the full elastic theory presented above, there is also a continuous and weak dependence of the results on the Poisson ratio of the elastic interior, but as long as the material remains somewhat compressible, these effects are subdominant.

It is of interest then to determine the expected magnitude of α for various systems of current interest. To do this, it convenient to rewrite this dimensionless quantity as the ratio of two lengths: $\alpha = R^3/\xi^3$, where the numerator is of purely geometric origin—the size of the sphere—and the denominator $\xi = (\kappa/\mu)^{1/3}$ is a length set by the ratio of the surface to bulk moduli of the system. For many soft polymeric gels and even for the interior of eukaryotic cells the typical values of the shear modulus are in the range of 10^2–10^4 Pa. Bending moduli of lipid bilayers are commonly found to be in the range of 10–100 k_BT at room temperature. This range of values generates a natural length scale of $\xi \sim 10^{-2}$–$10^{-1}\,\mu$m. Thus, for spheres of typical colloidal dimensions, $R \sim 1$–$10\,\mu$m, we find a range of $\alpha \sim 10^3$–10^9, justifying our focus on the large α regime. Since the optimally buckled state spherical harmonic $\ell^\star$ scales as $\alpha^{1/3}$, we predict that all buckled soft spheres of micron size will have $\ell^\star \sim \mathcal{O}(10)$. Such wrinkled states are indeed observed in the gel-filled vesicles [24]. We imagined that one encounters the mechanical instability leading to buckling via increasing the surface area of the bounding membrane at fixed interior volume. The gel-filled vesicle experiments generate the instability by reducing the interior at a fixed membrane surface area. Within linear elasticity theory as used here, these two approaches to the instability are equivalent. There may be biophysical examples of the same mechanical instability driven by membrane growth occurring in cells, nuclei, and, more broadly, during development.

It should be possible to extend this analysis to consider the dynamics morphological change in growing systems. We identify in our present work the requisite excess area for the morphological transition. As long as stress relaxation is fast compared to growth, our analysis remains valid for any growth model: Morphology is simply slaved to excess area. However, if one were to consider the interior to be viscoelastic with a sufficiently long stress relaxation time, then one should encounter interesting new dynamics of the instability by explicitly including material growth as explored in Refs. [13,37].

A similar buckling transition has been analyzed for the geometry of a thin shell or membrane on a flat elastic substrate [38]. In that work, the authors describe a critical buckling stress as opposed to a critical excess surface area, as we do. The two are simply related in linear elasticity theory. We find that our results may be equivalently described in terms of a critical stress in the membrane for buckling. The key distinction between buckling on a sphere and on a flat substrate is that the sphere's radius now enters the critical stress. We may, in fact, express that critical stress in terms of the control parameter α and a dimensionless function of the Poisson ratio of the internal material. The result is given in Appendix C.

Extending the above analysis to core-shell structures where the shell also contains a shear and area compression modulus remains an open and quite complex problem. We do expect the general phenomenology observed here to remain valid. Specifically, surface buckling will occur at a critical excess area and high moduli elastic interiors will push this morphological transition to lower critical fraction excess areas and require progressively lower symmetry buckled states for areas just above the critical value. We expect that the additional moduli associated with the surface will effectively stiffen the shell towards buckling and serve to further stabilize the isotropically extended sphere to larger values of Δ than those found here.

The theory presented here applies only for small distortions where linear elasticity remains valid. For the expected levels of fractional excess area $\Delta^\star \sim 0.5$ the typical size of the radial displacements at the surface are on the order of $u_r/R \sim 0.05$, so it seems reasonable to suppose that the application of the theory is valid up to the predicted morphological transition. Clearly, as more area is added beyond that point, nonlinear effects will become relevant. Numerical simulations [25] of elastic core-shell structures under "drying," where volume is removed from the interior rather than area added to the surface, have been performed. The results suggest that patterns reminiscent of those predicted here near the transition evolve under the further reduction of interior volume towards deeply folded surfaces where the folds meet in threefold junctions that roughly tessellate the surface. This suggests that elastic nonlinearities neglected here lead to fold formation, as might be expected based on the extensive work on folding of two-dimensional globally elastic [10] and flat elastica coupled to elastic or viscous subspaces [23]. Exploring the folding phenomenon and the interactions of folds on a curved surface remains an open problem.

ACKNOWLEDGMENTS

A.J.L. acknowledges enjoyable conversations with A. A. Evans and W. S. Klug. He also acknowledges partial support from NSF Grant No. DMR-1006162.

APPENDIX A: MODELING GROWTH VIA APPLIED STRESS

In our calculation we impose the excess area of the sphere's surface by applying constraint surface tractions as required to generate a specified radial displacement of the surface. The amplitude of that radial displacement is then determined by desired excess area. It is reasonable to ask whether such a procedure is equivalent to demanding the growth of the sphere's surface and then computing the elastic distortions required to accommodate that growth. In this appendix we demonstrate that, within a linear elastic theory, there is a simple correspondence between changes in the elastic reference state, reflecting material growth, and the application of constraint tractions at the boundary of the elastic object.

To begin, we consider the simplest case of one elastic degree of freedom. Imagine a single particle bound to the origin by a spring having spring constant k. Its energy of deformation in one dimension is

$$E = \frac{1}{2}kx^2, \tag{A1}$$

where x is the displacement of the particle. In this simple example, a change of reference state entails shifting the origin of the spring from $x = 0$ to $x = x_0$, yielding an energy function

$$E = \frac{1}{2}k(x - x_0)^2 = \frac{1}{2}kx^2 - F_0x + E_0, \tag{A2}$$

where $F_0 = kx_0$ and the constant in the energy $E_0 = \frac{1}{2}kx_0^2$ has no effect on the statics or dynamics of the system. From Eq. (A2) we see that the effect of shifting the reference state is equivalent to adding a constraint force F_0 to the original energy function for the unshifted spring in Eq. (A1).

We now consider a simplified one-dimension version of linear elasticity theory. We define the reference space labeling the undeformed mass points of the system by X on a segment of the x axis in the range [0,1]. We now grow this elastic material via the transformation $X \to \lambda X$, with $\lambda = 1 + \delta > 1$ for growth. In the original system displacement vectors $u = \mathbf{u} \cdot \hat{x}$ are defined in terms of the location of those same mass points in the deformed state by

$$u(X) = R(X) - X, \tag{A3}$$

where the mapping $X \to R(X)$ defines the deformation state of the one-dimensional elastic continuum. As expected from the global translational invariance of the energy, the energy density $e(X)$ of the elastic body is proportional to derivatives of the displacement vector with respect to the *reference state label* X. In the system with growth, this becomes

$$e(X) = \frac{1}{2}\mu\left(\frac{\partial}{\partial X}[R(X) - X - \delta X]\right)^2, \tag{A4}$$

where we have introduced a single elastic constant μ.

Expanding the square as we did for the simple spring system we find that the elastic energy density of deformation in the system with growth λ is given by

$$e(X) = \frac{1}{2}\mu\left(\frac{\partial u}{\partial X}\right)^2 - \sigma\frac{\partial u}{\partial X} + e_0, \tag{A5}$$

where $\sigma = \mu\delta$ now acts as a surface traction and the constant in the energy density is, once again, physically irrelevant. Thus, we see in a one-dimensional model of linear elasticity, growth of the reference state is identical mechanically to applying the appropriate set of surface tractions. In our calculation, we did not know these tractions *a priori* but determined them later by required a fixed increase in the surface area of the growing and elastically deformed structure.

The principle demonstrated here applies for three-dimensional vectorial displacements at the cost of some trivial complexity involving indices. Note that the equivalence exploited here is valid only if one assumes a linear elastic material for which all terms in the energy functional are quadratic in the strain tensor. It is only in this case that expanding the square generates a linear shift in the energy interpreted as the surface traction and an irrelevant additional constant. Future studies of nonlinear elastic systems will require a more sophisticated approach to the problem of changing the reference state of the material.

APPENDIX B: SOLVING FOR THE ELASTIC DEFORMATION OF THE SPHERE'S INTERIOR

In this appendix we examine in more detail the solution to elasticity problem proposed in the text. Namely, if one were to specify a radial displacement of the surface of an elastic sphere in terms of a single spherical harmonic, what is the form of the displacement field in the sphere's interior? We solved this problem by asserting that one may find a harmonic vector field $\mathbf{S}_{\ell m}$ that satisfies the required radial displacements on the sphere's surface. In this appendix we present some of the details of that computation and give the solution of the displacement field $\mathbf{u}(\mathbf{x})$.

On the surface of the sphere we require the vector field $\mathbf{S}_{\ell m}$ to be given by

$$\mathbf{S}_{\ell m} = g_{\ell m}\hat{r}Y_{\ell m}. \tag{B1}$$

To construct a harmonic vector of this form we write the Cartesian components of this vector field at the surface, expand these components in sums of spherical harmonics, and then multiple each of them the appropriate factor of $(r/R)^\ell$ to make these function harmonic in the interior. These x,y,z Cartesian components are then of the form $Y_{\ell m}\sin(\theta)\cos(\phi)$, $Y_{\ell m}\sin(\theta)\cos(\phi)$, $Y_{\ell m}\cos\theta$, respectively. Using the usual rules for the addition of angular momentum, these products can be expanded in sums of other spherical harmonics. Specifically, we may use the fact that the product of two spherical harmonics may be expanded in terms of a sum of spherical harmonics using the Wigner $3-j$ symbols,

$$Y_{\ell_1}^{m_1}Y_{\ell_2}^{m_2} = \sum_{\ell m}\sqrt{\frac{(2\ell_1+1)(2\ell_2+1)(2\ell+1)}{4\pi}} \times \begin{pmatrix} \ell_1 & \ell_2 & \ell \\ m_1 & m_2 & m \end{pmatrix} Y_\ell^{-m} \begin{pmatrix} \ell_1 & \ell_2 & \ell \\ 0 & 0 & 0 \end{pmatrix}. \tag{B2}$$

The Wigner $3-j$ symbols are simply related to the better-known Clebsch-Gordan coefficients. The reader may refer to any standard reference on quantum mechanics [39,40]. In the products above, ℓ_1,m_1 refer to the angular harmonic of the imposed surface deformation and ℓ_2,m_2 to the decomposition of the radial unit vector into its Cartesian components. Thus, $\ell_2 = 1$ and $m_2 = \pm 1,0$. Given this simplification, it is useful to define $A_\pm^{\pm,0}$, where the lower indices refer an increase or decrease of the total angular momentum, $\ell \to \ell \pm 1$, while the upper index refers to the change in its z-axis projection, $m \to m \pm 1,m$,

$$A_-^{\pm}(\ell,m) = \frac{-1}{2}\sqrt{\frac{3}{2\pi}}\sqrt{\frac{(\ell \mp m - 1)(\ell \mp m)}{(2\ell-1)(2\ell+1)}}, \tag{B3}$$

$$A_+^{\pm}(\ell,m) = \frac{1}{2}\sqrt{\frac{3}{2\pi}}\sqrt{\frac{(\ell \pm m + 2)(\ell \pm m + 1)}{(2\ell+1)(2\ell+3)}}, \tag{B4}$$

for the terms generating m values of $m \pm 1$ and

$$A_{-}^{0}(\ell,m) = \sqrt{\frac{3}{4\pi}}\sqrt{\frac{(\ell^2-m^2)}{(2\ell-1)(2\ell+1)}}, \tag{B5}$$

$$A_{+}^{0}(\ell,m) = \sqrt{\frac{3}{4\pi}}\sqrt{\frac{(\ell+m+1)(\ell-m+1)}{(2\ell+1)(2\ell+3)}}, \tag{B6}$$

for the terms with the same m value as the radial surface deformation.

At this point it is useful to define $Y_{\ell m}$ for $m < 0$,

$$Y_{\ell m} = \tfrac{1}{i\sqrt{2}}\left[Y_{\ell}^{|m|} - (-1)^m Y_{\ell}^{-|m|}\right] \quad m < 0. \tag{B7}$$

This is simply a rotation of the $Y_{\ell|m|}$ mode through an angle $\phi_0 = \frac{\pi}{2m}$. Defining $Y_{\ell m}$ for all $m \in \mathbb{I}$ allows us to describe a mode rotated by any angle. This notation is useful in the Cartesian representation of the deformation field.

Using this decomposition of the $\mathbf{S}_{\ell m}$ vector into its spherical harmonic components, multiplying each by the appropriate power $(r/R)^{\ell}$ to make this vector field harmonic in the sphere's interior, and using the above notation, we find

$$\begin{aligned} S_x = \mathrm{Sgn}(m) g_{\ell m}\sqrt{\frac{2\pi}{3}}\Bigg\{&\left(\frac{r}{R}\right)^{\ell-1}\left[A_{-}^{-}(\ell,m)(1-2\delta_{m,0})Y_{\ell-1,m-1} - A_{-}^{+}(\ell,m)(1-\delta_{m,-1})Y_{\ell-1,m+1}\right] \\ &+\left(\frac{r}{R}\right)^{\ell+1}\left[A_{+}^{-}(\ell,m)(1-2\delta_{m,0})Y_{\ell+1,m-1} - A_{+}^{+}(\ell,m)(1-\delta_{m,-1})Y_{\ell+1,m+1}\right]\Bigg\}, \end{aligned} \tag{B8}$$

$$\begin{aligned} S_y = -\mathrm{Sgn}(m) g_{\ell m}\sqrt{\frac{2\pi}{3}}\Bigg\{&\left(\frac{r}{R}\right)^{\ell-1}\left[A_{-}^{-}(\ell,m)Y_{\ell-1,-m-1} + A_{-}^{+}(\ell,m)Y_{\ell-1,-m+1}\right] \\ &+\left(\frac{r}{R}\right)^{\ell+1}\left[A_{+}^{-}(\ell,m)Y_{\ell+1,-m-1} - A_{+}^{+}(\ell,m)Y_{\ell+1,-m+1}\right]\Bigg\}, \end{aligned} \tag{B9}$$

$$S_z = g_{\ell m}\sqrt{\frac{4\pi}{3}}\left\{\left(\frac{r}{R}\right)^{\ell-1} A_{-}^{0}(\ell,m)Y_{\ell-1,m} + \left(\frac{r}{R}\right)^{\ell+1} A_{+}^{0}(\ell,m)Y_{\ell+1,m}\right\}, \tag{B10}$$

where we have written the result in terms of the real spherical harmonics defined in the text so each term of the above harmonic vector is explicitly real. Finally, we have introduced the *sign function* $\mathrm{Sgn}(x) = +1$ for non-negative x and -1 otherwise.

Finally, for completeness, we record the Cartesian components of the displacement vector field $\mathbf{u}(\mathbf{x})$ for a given radial deformation field on the sphere's surface taken to be a single (real) spherical harmonic,

$$\begin{aligned} u_x = g_{\ell m}\frac{r^{\ell-1}}{4R^{\ell+1}}\Bigg[&\left(2r^2\sqrt{\frac{1}{(4\ell^2-1)}} - \frac{(R^2-r^2)(\ell-4\nu+5)\sqrt{\frac{(2\ell+1)}{(2\ell-1)}}}{\ell(4\nu-3)+2\nu-1}\right) \\ &\times\left(\sqrt{(\ell-m-1)(\ell-m)}Y_{\ell-1,m+1} - \mathrm{Sgn}(m-1)^{m-1}\sqrt{(\ell+m-1)(\ell+m)}Y_{\ell-1,|m-1|}\right) \\ &-2r^2\sqrt{\frac{2\pi}{3}}\left(A_{+}^{+}(\ell,m)Y_{\ell+1,m+1} - \mathrm{Sgn}(m-1)^{m-1}\,A_{+}^{-}(\ell,m)Y_{\ell+1,|m-1|}\right)\Bigg], \end{aligned} \tag{B11}$$

$$\begin{aligned} u_y = g_{\ell m}\frac{r^{\ell-1}}{4R^{\ell+1}}\Bigg[&\left(2r^2\sqrt{\frac{1}{(4\ell^2-1)}} - \frac{(R^2-r^2)(\ell-4\nu+5)\sqrt{\frac{(2\ell+1)}{(2\ell-1)}}}{\ell(4\nu-3)+2\nu-1}\right) \\ &\times\left(\sqrt{(\ell-m-1)(\ell-m)}Y_{\ell-1,m-1} + \mathrm{Sgn}(m-1)^{m}\sqrt{(\ell+m-1)(\ell+m)}Y_{\ell-1,-|m+1|}\right) \\ &-2r^2\sqrt{\frac{2\pi}{3}}\left(A_{+}^{-}(\ell,m)Y_{\ell+1,m-1} + \mathrm{Sgn}(m-1)^{m}\,A_{+}^{+}(\ell,m)Y_{\ell+1,-|m+1|}\right)\Bigg], \end{aligned} \tag{B12}$$

$$u_z = g_{\ell m}\frac{r^{\ell-1}}{R^{\ell+1}}\sqrt{\frac{4\pi}{3}}\left[r^2 A_{+}^{0}Y_{\ell+1,m} + A_{-}^{0}\frac{(2\ell^2+5\ell+3)r^2 - (2\ell+1)R^2(\ell-4\nu+5)}{2(\ell(4\nu-3)+2\nu-1)}Y_{\ell-1,m}\right]. \tag{B13}$$

This completes the analysis of the displacement field inside the elastic sphere when a radial deformation whose amplitude is proportional to a single spherical harmonic is imposed on the surface.

APPENDIX C: CRITICAL STRESS FOR BUCKLING

One may calculate the critical surface stress required for the morphological transition using the elastic theory. We calculate the critical stress by computing the surface stress of the $\ell = 0$ mode as a function of g_{00}. We then use the critical fractional excess area $\Delta^\star$ to solve for the value of g_{00} at the buckling transition.

The critical stress may be written in terms of the control parameter α, κ/R^3, and a dimensionless function of ν, the Poisson ratio of the interior. This function $f(\nu)$ is difficult to produce in closed form, but we find that the following polynomial serves as a good numerical approximation for $\nu \geqslant 0$:

$$f(\nu) = -7.92208\nu^3 + 10.2125\nu^2 - 9.19217\nu + 3.0332. \tag{C1}$$

In terms of this function the critical stress $\sigma^\star$ is given by

$$\sigma^\star = \frac{\kappa}{R^3}\frac{(1+\nu)\sqrt{2/\pi}}{1-2\nu}\left(\frac{f(\nu)\alpha^{2/3}}{2} - \frac{f^2(\nu)\alpha^{1/3}}{8}\right). \tag{C2}$$

[1] L. Euler, *Mechanica, Sive Motus Scientia Analytice* (Ex Typographia Academiae Scientiarum, St. Petersburg, Russia, 1736).
[2] L. Landau and E. Lifshitz, *Theory of Elasticity*, Vol. 7 of Course of Theoretical Physics, 3rd ed. (Elsevier, Amsterdam, 1986).
[3] L. Golubović, D. Moldovan, and A. Peredera, Phys. Rev. Lett. **81**, 3387 (1998).
[4] J. D. Hartog, *Strength of Materials* (Dover, New York, 1977).
[5] M. Das, A. Levine, and F. MacKintosh, Europhys. Lett. **84**, 18003 (2008).
[6] O. Chaudhuri, S. Parekh, and D. A. Fletcher, Nature **445**, 295 (2007).
[7] E. Conti and F. C. MacKintosh, Phys. Rev. Lett. **102**, 088102 (2009).
[8] M. S. e Silva, M. Depken, B. Stuhrmann, M. Korsten, F. MacKintosh, and G. H. Koenerink, Proc. Natl. Acad. Sci. USA **108**, 9408 (2011).
[9] D. R. Nelson and L. Peliti, J. Phys. **48**, 1085 (1987).
[10] E. Cerda and L. Mahadevan, Phys. Rev. Lett. **90**, 074302 (2003).
[11] E. Rodriguez, A. Hoger, and A. McCulloch, J. Biomech. **27**, 455 (1994).
[12] D. Drasdo, Phys. Rev. Lett. **84**, 4244 (2000).
[13] A. Goriely and M. Ben Amar, Phys. Rev. Lett. **94**, 198103 (2005).
[14] J. Dervaux and M. Ben Amar, Phys. Rev. Lett. **101**, 068101 (2008).
[15] A. N. M. Kücken, Europhys. Lett. **68**, 141 (2004).
[16] T. Sato, R. G. Vries, H. J. Snippert, M. van de Wetering, N. Barker, D. E. Stange, J. H. van Es, A. Abo, P. Kujala, P. J. Peters, and H. Clevers, Nature **459**, 262 (2009).
[17] E. Hannezo, J. Prost, and J. F. Joanny, Phys. Rev. Lett. **107**, 078104 (2011).
[18] J. Genzer and J. Groenewold, Soft Matter **2**, 310 (2006).
[19] J. Yoon, J. Kim, and R. C. Hayward, Soft Matter **6**, 5807 (2010).
[20] D. Breid and A. J. Crosby, Soft Matter **7**, 4490 (2011).
[21] M. Trejo, C. Douarche, V. Bailleux, C. Poulard, S. Mariot, C. Regeard, and E. Raspaud, Proc. Natl. Acad. Sci. USA **110**, 2011 (2013).
[22] R. Huang and S. Im, Phys. Rev. E **74**, 026214 (2006).
[23] H. Diamant and T. A. Witten, Phys. Rev. Lett. **107**, 164302 (2011).
[24] A. Viallat, J. Dalous, and M. Abkarian, Biophys. J. **86**, 2179 (2004).
[25] B. Li, F. Jia, Y.-P. Cao, X.-Q. Feng, and H. Gao, Phys. Rev. Lett. **106**, 234301 (2011).
[26] A. C. Rowat, J. Lammerding, and J. H. Ipsen, Biophys. J. **91**, 4649 (2006).
[27] C. Brangwynne, F. MacKintosh, S. Kumar, N. Geisse, J. Talbot, L. Mahadevan, K. K. Parker, D. E. Ingber, and D. Weitz, J. Cell Biol. **173**, 733 (2006).
[28] S. Safran, *Statistical Thermodynamics of Surfaces, Interfaces, and Membranes*, Frontiers in Physics (Westview Press, Boulder, CO, 2003).
[29] S. T. Milner and S. A. Safran, Phys. Rev. A **36**, 4371 (1987).
[30] P. Leo, J. Iwan, D. Alexander, and R. Sekerka, Acta Metallurgica **33**, 985 (1985).
[31] J. D. Finan and F. Guilak, J. Cell. Biochem. **109**, 460 (2010).
[32] G. Cao, X. Chen, C. Li, A. Ji, and Z. Cao, Phys. Rev. Lett. **100**, 036102 (2008).
[33] A. C. Rowat, D. Keller, and J. H. Ipsen, Biochim. Biophys. Acta **1713**, 29 (2005).
[34] J. Yin, Z. Cao, C. Li, I. Sheinman, and X. Chen, Proc. Natl. Acad. Sci. USA **105**, 19132 (2008).
[35] H. Shum, E. Santanach-Carreras, J.-W. Kim, A. Ehrlicher, J. Bibette, and D. A. Weitz, J. Am. Chem. Soc. **133**, 4420 (2011).
[36] B. a. Mattson, E. W. Overstrom, and D. F. Albertini, Biol. Reprod. **42**, 195 (1990).
[37] M. Ben Amar and A. Goriely, J. Mech. Phys. Solids **53**, 2284 (2005).
[38] X. Chen and J. Hutchinson, J. Appl. Mech. **71**, 597 (2004).
[39] E. U. Condon and G. H. Shortley, *The Theory of Atomic Spectra* (Cambridge University Press, Cambridge, 1935).
[40] A. Messiah, *Quantum Mechanics* (Dover, London, 1999).